Analysis of Power and Torque for the IPM Motors with High Flux Density in Stator

Vuong DANG QUOC[1], *Dinh BUI MINH*[1], *Phi DO CHI*[2], *Hung BUI DUC*[1]

[1]School of Electrical Engineering, Hanoi University of Science and Technology,
No.1, Dai Co Viet Street, Hai Ba Trung District, Hanoi, Vietnam
[2]Engineering Cao Thang Technical College,
65 Huynh Thuc Khang Street, Ben Nghe Ward, District 1, Ho Chi Minh city, Vietnam

vuong.dangquoc@hust.edu.vn, dinh.buiminh@hust.edu.vn, dochiphi@caothang.edu.vn,
hung.buiduc@hust.edu.vn

DOI: 10.15598/aeee.v21i2.4817

Article history: Received Nov 03, 2022; Revised Jun 13, 2023; Accepted Jun 18, 2023; Published Jun 30, 2023.

Abstract. *The new idea of this paper is to focus on investigating the influence of characteristics on the power and torque of an Interior Permanent Magnet (IPM) motor designed by the Tesla rear-drive. The detail of improvement designs of double V (2V) shape and inverter delta (VI) shape has been proposed for electric vehicles taking a high constant torque in a wide range speed into account. The torque ripple, output power and torque density are developed and evaluated in different topologies via the finite element method. The two-layered rotor structure with the 2V and VI shapes is also designed to give the suitable choices for manufacturing in mass production. For the higher torque density and efficiency, the two-layered 2V or VI magnets of IPM motor with 72 slots/ 8 poles can be adjusted with the sinusoidal step skewing to minimize the torque ripple, harmonic components and back electromotive force. The developed method is performed on the practical problem of the IPM motor of 200 kW −450 Nm, which is applied to the single drive system delivers.*

Keywords

Back Electromagnetic Force (EMF), double V (2V) and VI shapes, Finite Element Method (FEM), high flux density, IPM motor, torque ripple.

1. Introduction

The Lucid Air sedan is known as a high-end luxury electric car with an astounding 805 kW. It can be obtained from 465 to 503 miles of range in its top Dream Edition specification [1] and [2]. The rear and front suspension wheels allow them to be combined together, and in particular based on the compact nature of these modules, additional motors can be accommodated. The power and the potential for advanced torque can be improved by using the rotor shape of double V (2V) and VI magnet designs. In addition, the associated components of electric motors are capable of delivering up to 499 kW apiece, which can be touched on the new Electric Vehicle (EV) of the trick powertrain layout back. However, for the high output powers of the Dream Edition, it gets two motors of 805 kW and 193.8 kW. The lower power levels are designed to get output powers with a range of 298 kW, 462 kW, and 596.5 kW, all of which are considered as the dual motor, so getting even more untapped potential.

Many different approaches have been studied for improving electromagnetic parameters of the IPM motor as introduced in the literature [8], [9], [10], [11] and [12]. In reference [11], a nonlinear switching feedback element was incorporated into the prediction equation to address the model uncertainties, disturbances, and variations in motor characteristics. This approach helps to reduce harmonic distortion and torque ripple. In reference [12], the Modified Brain Emotional Controller (MBEC) technique was proposed to minimize torque and flux ripples in sensorless Direct

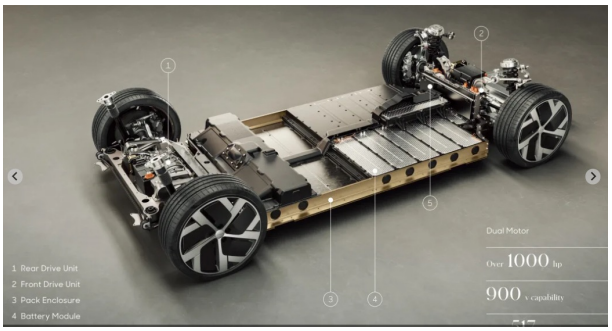

Fig. 1: Lucid air powertrain [2].

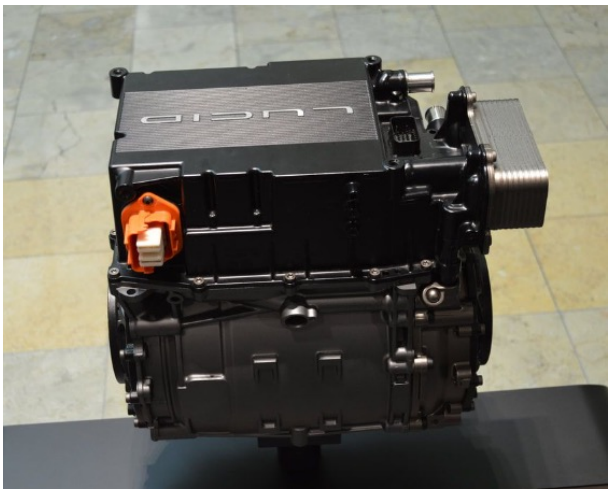

Fig. 2: Lucid air powertrain [2].

Torque Control (DTC) technique. This technique utilized a biologically inspired intelligent speed controller to enhance the system performance. In reference [13], a finite-element analysis was presented to investigate and compare the electromagnetic performance of three different multi-layered IPM machines for use in electric vehicles. The rotor structure, air-gap field distribution, torque density, torque ripple, core loss, magnet eddy-current loss, and output power were also analysed. Reference in [14], the improvement in torque ripple was estimated by the optimized stator flux selection. The development of the method was considered with both steady-state and dynamic operating conditions. Reference in [15], the paper focused on analysing the rotor shapes of IPM motors for electric vehicles. The authors analysed five different types of motor rotors, including two hybrid vehicles, to compare their torque, torque ripple, efficiency, and back-electromotive voltage. To minimize the number of variables in the analysis, the size of the motor stators was fixed, and only the rotor shapes were modified. The new idea of this paper is to consider a used vehicle part market to analyse and simulate. In order to rebuild the motor geometry via the Finite Element (FEM) model, a tear-down of the motor (Fig. 1) is performed to analyse the motor components from the rest of the drive system. The subject motor is employed in the Lucid Airrear-drive unit is pointed out in Fig. 2. The single drive system delivers of power from 190 kW to 211 kW, for the torque from 420 Nm to 450 Nm are presented in this study [2] and [3]. The FEM associated with Motor-CAD software to investigate and analyse the characteristics and performance of motors. The stator and rotor assemblies of the motor has been further separated to reveal. In order to improve the ripple torque and efficiency, the hairpin windings are presented to replace the distributed winding forms. The stator parameters are depicted in Fig. 3. The drawing of rotor magnet of the Lucid Air electric motor is presented in Fig. 4.

The main parameters of the rotor lamination sheet and the magnet are measured as shown in Fig. 5. It should be noted that the four segments inserted in the magnet do not form as a Halbach array. Both sides of the magnet have been evenly measured with the same magnetic field. Based on the segmentation of the magnet, it allows to reduce the eddy current distribution in iron cores of the electric motors. The detailed results obtained from the tear-down are then imported in the MotorXP Design Studio. The important parameters such as windings, rotor skew are manually import to complete the problem procedure. The complete process will be presented in the next Section.

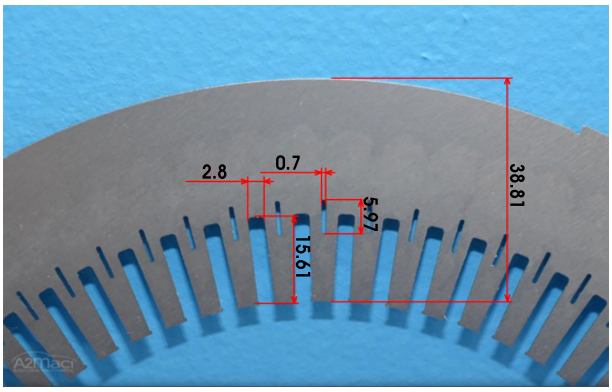

Fig. 3: Drawing of stator.

The characteristics of the motor can be also examined by the magnetostatic problem. Thus, beside the information of voltage, current, torque and loss, other quantities can be extracted from this problem too. For example, the distribution of magnetic flux density can be simulate/computed to indicate that the motor is not saturated during operation. This aims to present the distribution of magnetic flux density at different parts. This also predicts the safety and efficiency of the motor by increasing torque and current accordingly.

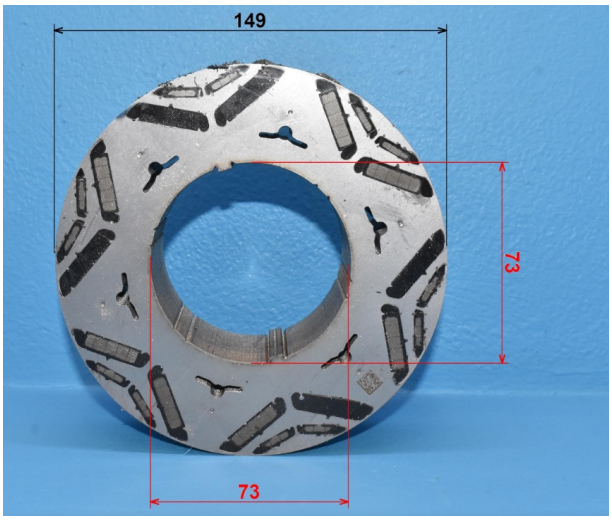

Fig. 4: Drawing of rotor permanent magnet.

2. Electromagnetic Design of 2V and VI Topologies

The improvement proposals of IPM motor are designed via an existing IPM motor of 210 kW, for a peak power of 450 Nm, and 18,000 rpm. The main geometry parameters of the improvement IPM is given in Tab. 1.

The main parameters of IPM motor, such as poles, slots, diameters of stator and rotor, stack length and the air-gap length are given in Tab. 1. These parameters are designed for the continuous rated power of IPM motor of 190 kW, maximum speed of 18,000 rpm and the power inverter of 450 VDC/500 A. An embedded permanent magnet for the rotor configuration is designed as the main part of the process.

By using an analytical program, it is developed to estimate the radial force via a Matlab tool coupling to the FEM as presented in Fig. 6. The program is split into three main parts, where the analytical calculation is first considered to define main parameters of the proposed machine, the obtained result will be then exported as drawings. Finally, the FEM simulation is proposed for coupling to Matlab.

Tab. 1: GLCM arrays with different offsets and directions.

No.	Parameters	Values	Unit
1	Slot number	72	-
2	Stator lamination diameter	230	mm
3	Stator Bore	112	mm
4	Tooth width	4.15	mm
5	Motor length	150	mm
6	Slot depth	21.1	mm
7	Rotor lamination length	150	mm
8	Stator lamination length	150	mm
9	Magnet length	150	mm
10	Airgap	80.75	mm
11	Pole number	8	mm

In this structure, the voltage-limit circle is a current locus defining all possible currents that can be obtained when the inverter voltage is limited, rather than its current. Let V_m be the maximum available supply voltage per phase. The voltage to each phase of the motor is supplied by an inverter, such that the phase angle between V_m and E is γ (Fig. 7). The current and voltage are then calculated as [4], [5] and [6]:

$$I_q = \frac{V_q - E}{X_q} = \frac{V_q \cos\gamma - E}{X_d}, \tag{1}$$

$$I_d = \frac{-V_d}{X_q} = \frac{V_q \sin\gamma - E}{X_q}, \tag{2}$$

$$V_m^2 = V_d^2 + V_q^2, \tag{3}$$

$$(X_q I_q)^2 = (E + X_d I_d)^2 = V_m^2, \tag{4}$$

where V_d and V_q are respectively the direct and quadrature axis voltage; I_d and I_q are the direct and quadrature axis currents, respectively; X_q and X_d are respectively the quadrature and direct axis reactances.

This is an ellipse in the plane of $X_d = X_q$, and I_d and I_q, where the voltage-limit ellipse is a circle (Fig. 8). Note that E/X_d is the short-circuit current, which is normally a large current, so that the point C normally lies outside the current-limit circle, while the short-circuit current E/X_d remains constant. Consequently, when the speed increases, the ellipse or voltage-limit circle can shrinks. At certain values of the voltage to maintain the current I_m, which becomes a limited voltage. This condition is associated with "saturation" of the regulated current, which is checked to be lose to a control of the current waveform [7], [8] and [9]:

$$\left(\frac{V_m}{X_q}\right)^2 = \left(\frac{V_m}{X_q}\right)^2 + I_m^2, \tag{5}$$

$$\omega = \frac{V_m}{\sqrt{\psi_{1Md}^2 + (L_d I_m)^2}}. \tag{6}$$

For the current-limited maximum torque (Fig. 10), the electromagnetic torque (T_e) can be computed via the phase angle γ, E and V_m [8] and [10], i.e.:

$$T_e = mp\left[\psi_{1Md} I \cos\gamma - I^2 \sin\gamma\cos\gamma\,(L_d - L_q)\right], \tag{7}$$

When the current I is a constant, the torque will be obtained as a maximum value with the γ:

$$\gamma_{T_{\max}} = \sin^{-1}\frac{1}{4}\left[-\frac{\psi_{1Md}}{\Delta\psi} + \sqrt{\left(\frac{\psi_{1Md}}{\Delta\psi}\right)^2 + 8}\right]. \tag{8}$$

In addition, the torque can be defined by X_d and X_q with the variable of γ between V_m and E, that is:

$$T_e = \frac{mp}{w}\left[\frac{EV_m}{X_d}\sin\gamma + \frac{V_m^2}{2}\left(\frac{1}{X_q} - \frac{1}{X_d}\right)\sin 2\gamma\right]. \tag{9}$$

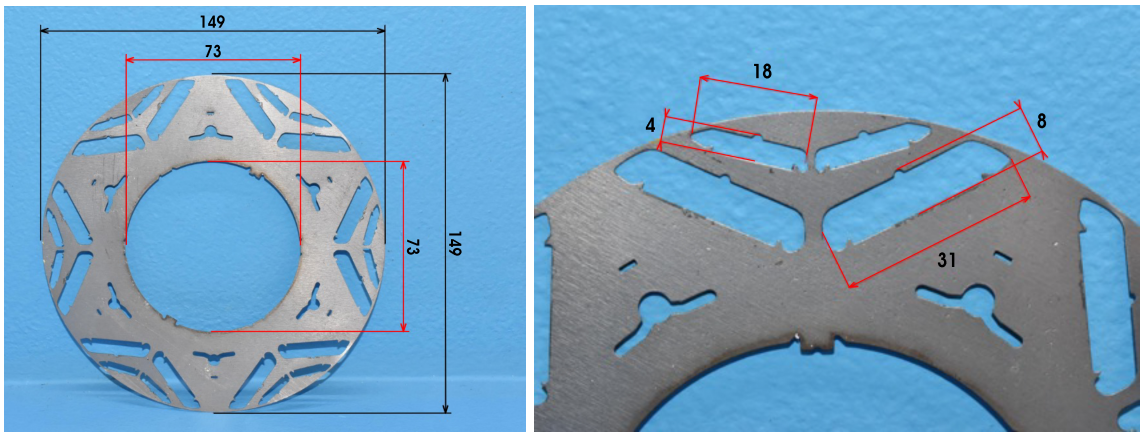

(a) (b)

Fig. 5: Lamination model of rotor.

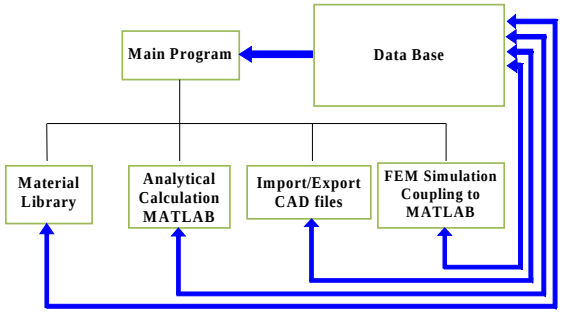

Fig. 6: Analytical program structure.

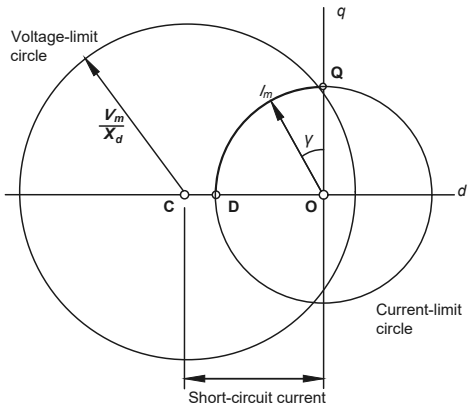

Fig. 7: Current and voltage-limit circle at the change-over speed; non-salient-pole motor with $X_d = X_q$.

The phase angle γ with the maximum torque is defined as [8] and [10]:

$$\gamma_{T_{\max}} = \cos^{-1}\left[\left(-\varsigma \pm \frac{\sqrt{\varsigma^2+8}}{4}\right)\right], \tag{10}$$

where ς is expressed as:

$$\varsigma = \frac{X_q E}{V_m\,(X_q - X_d)}. \tag{11}$$

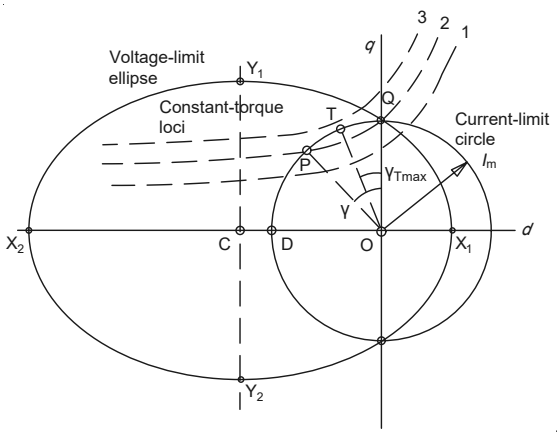

Fig. 8: Current and voltage-limit circle at the change-over speed; non-salient-pole motor with $X_d = X_q$.

A locus of constant-torque is superimposed on the circle diagram via the expression:

$$T_e = mp\,[\psi_{1Md} - I\sin(L_d - L_q)]\,I\cos\gamma. \tag{12}$$

As γ increases from zero, the reluctance term $I\sin\gamma$ increases quickly while $\cos\gamma$ changes only slowly. Although the alignment torque is decreasing, the reluctance torque is increasing at a faster rate, until γ reaches $\delta_{T_{max}}$. In terms of EMF and reactances, it has [8] and [10]:

$$T_e = \frac{mp}{w}[E - I\sin\delta(X_d - X_q)]I\cos\gamma. \tag{13}$$

It can be also used to define the phase angle $\delta_{T_{max}}$ in advance. For that, the maximum torque for any given value of current can be obtained. For a non-salient pole motor, it is a simple problem to adapt this to X_d and X_q. Two the proposed Permanent Magnet Assisted Synchronous Reluctance Motors (PMA-SynRM) are given in Tab. 2.

Tab. 2: Efficiency comparison of Model 2V and VI.

Parameters	2V	VI	Unit
Torque ripple	17.734	230	Nm
Average torque	161.63	13.19	Nm
Torque ripple (%)	10.949	7.6935	%
Cogging torque ripple	2.4068	5.6558	Nm
Input Power	172	181	kW
Total losses	5.767	6.284	kW
System Efficiency	96.639	96.837	%
Shaft Torque	158.33	167.3	Nm
Armature DC copper loss	1.951	1.951	kW
Magnet loss	0.1453	0.006	kW
Stator iron loss	3.521	3.935	kW
Rotor iron loss	0.256	0.248	kW
Total losses	5.767	5.685	kW

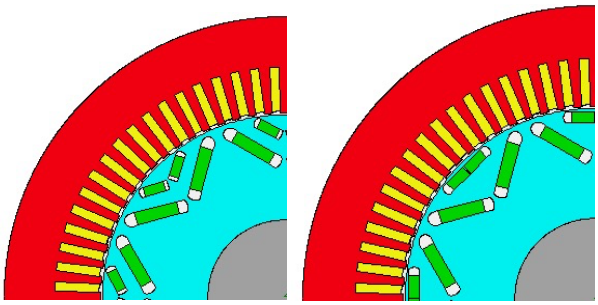

Fig. 9: Constant-torque loci.

In order to verify the electromagnetic performances of a 48 slots/8 poles proposed IPMs, the 2V and VI shape topologies are presented in Fig. 9. The back Electromotive Forces (EMFs) and torque are simulated by the FEM. The obtained results have shown that the delta shape has a lower torque ripple, and harmonic components of the back EMF are neglected. The distributions of magnetic flux density for the different parts is pointed in Fig. 10. The obtained results have shown that the investigated motor is not saturated during operation.

This aims to predict the efficiency of the motor by increasing torque and current accordingly. The comparison of torque ripple, the back EMF and efficiency for two models (2V and IV shapes) are presented in Fig. 11, Fig. 12and Fig. 13, respectively.

It can be seen that the torque ripple for the VI model are relatively improved compared to the 2V model, and the back EMF waveform is smoothly distributed. A power inverter of 450 VDC/300 A has been supplied to the PMa-SynRM to verify the rated power and torque as shown in Fig. 14 and Fig. 15. In Fig. 14, at the speed of 15,000 rpm, the output power for the VI model is 172 kW, being 8.8 % higher than that of the 2V model of 156 kW, because the permanent magnet is arranged closer to the air gap.

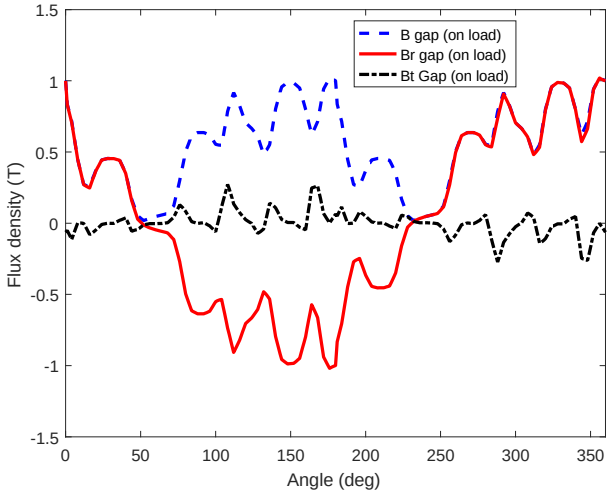

Fig. 10: Topology of 2V and VI shapes.

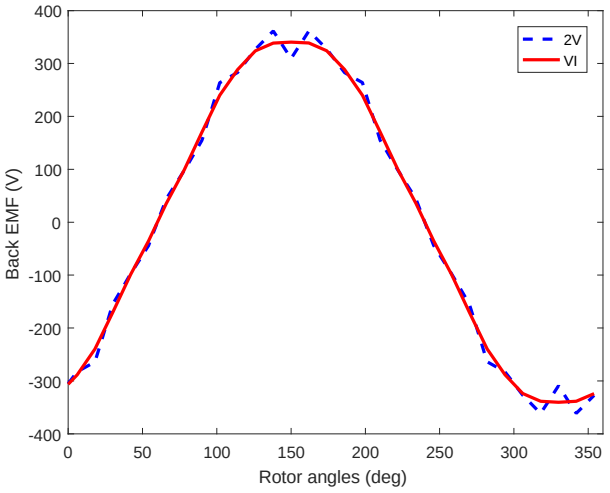

Fig. 11: Distribution of magnetic flux density on the different parts of motor with the VI shape.

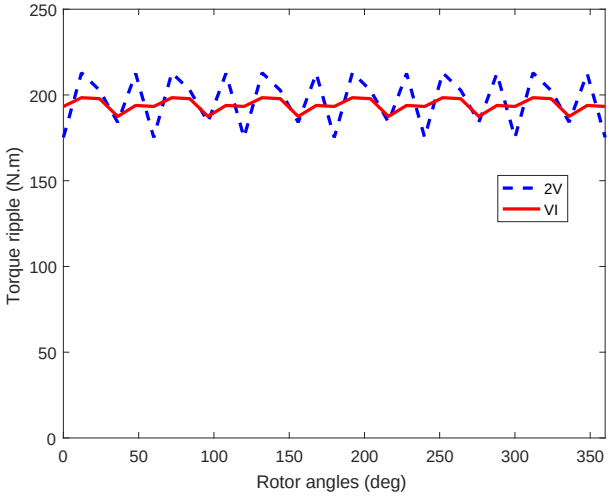

Fig. 12: Comparison of torque ripple for 2V and IV shapes.

Hence, the flux density is increased. In Fig. 15, the rated torque for the VI model is about 110 Nm, which

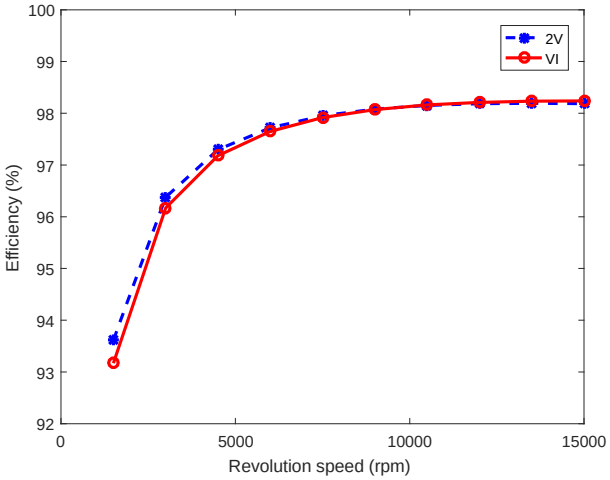

Fig. 13: Comparison of efficiency of 2V and VI shapes.

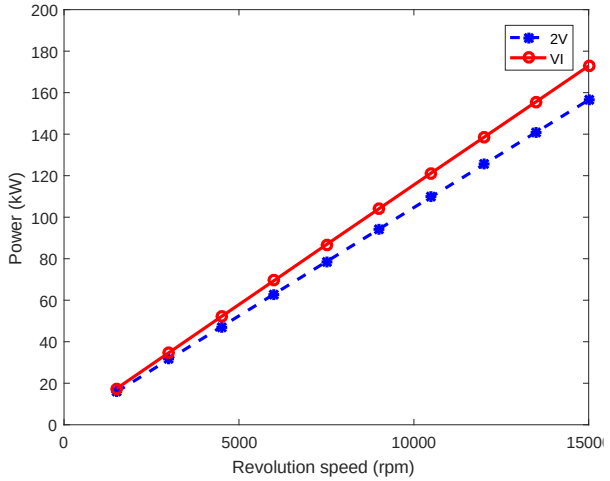

Fig. 14: Comparison of rated power of 2V and VI shapes.

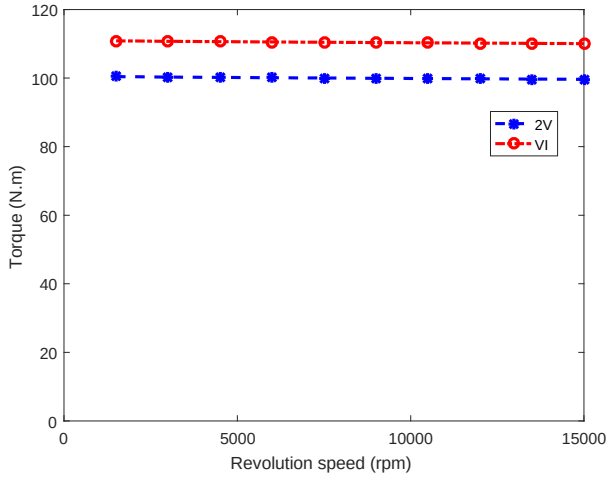

Fig. 15: Comparison of rated torque of 2V and VI shapes.

is bigger for about 13.8 % in comparison with the 2V model of 96.6 Nm. The extreme difference between the 2V and VI variant in the calculation of torques is that the analytical model for 2V and VI calculation is applied for electromagnetic equations to adjust parameters for the 2V and VI magnet arrangements which have been programed in MATLAB program coupling to CAD and FEM methods. Finally, the motor assembly is shown in Fig. 16.

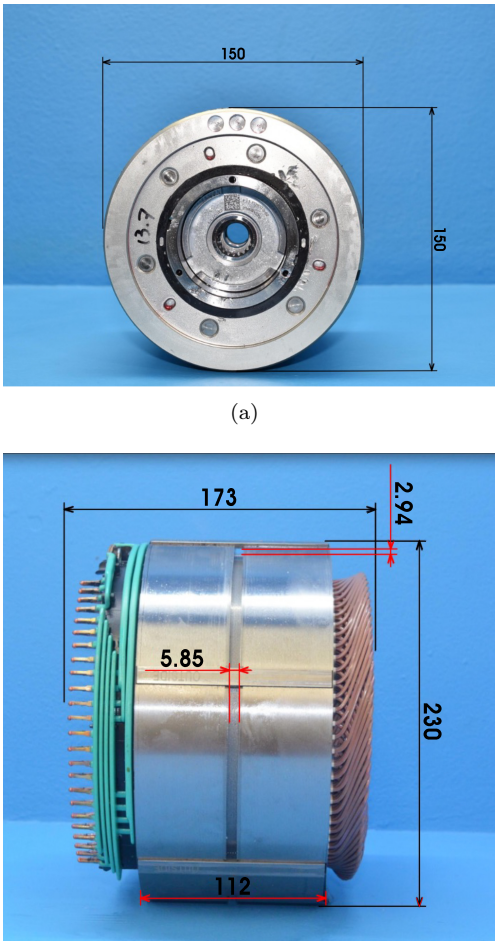

(a)

(b)

Fig. 16: Modeling of motor after assemblying.

3. Conclusion

The electromagnetic parameters of the IPM motors such as the torque ripple, back EMF, efficiency, rated power and rated torque with different 2V and VI shapes have been successfully presented. The obtained results have shown that the VI shape has superior performances compared to the 2V shape, such as a higher efficiency, power and torque due to a combination of an optimal V angle and I simplicity, which helps to decrease harmonic distortions in the air-gap density. In particular, the VI shape has been used to improve the back EMF and torque ripple of the Lucid AirMotor as shown in Fig. 16. These findings suggest that the VI shape can be a promising solution for improving the performance of IPM motors in various applications.

Acknowledgment

This research is funded by Hanoi University of Science and Technology under project number T2022-PC-009.

Author Contributions

V.D.Q. and D.B.M. developed the proposed model with the different topologies (2V and VI shapes). H.B.D. applied the analytic approach to compute electromagnetic parmeters of the IPM motor. P.D.C. simulated the IPM motor by the FEM. All authors contributed to the final version of the manuscript.

References

[1] HUYNH, T. A. and M.-F. HSIEH. Performance Analysis of Permanent Magnet Motors for Electric Vehicles (EV) Traction Considering Driving Cycles. *Energies*. 2018, vol. 11, iss. 6, pp. 1–24. ISSN 1996-1073. DOI: 10.3390/en11061385.

[2] CAO, R., C. MI and M. CHENG. Quantitative Comparison of Flux-Switching Permanent-Magnet Motors With Interior Permanent Magnet Motor for EV, HEV, and PHEV Applications. *IEEE Transactions on Magnetics*. 2012, vol. 48, iss. 8, pp. 2374–2384. ISSN 1941-0069. DOI: 10.1109/TMAG.2012.2190614.

[3] WU, W., X. ZHU, L. QUAN, Y. DU, Z. XIANG and X. ZHU. Design and Analysis of a Hybrid Permanent Magnet Assisted Synchronous Reluctance Motor Considering Magnetic Saliency and PM Usage. *IEEE Transactions on Applied Superconductivity*. 2018, vol. 28, iss. 3, pp. 1–6. ISSN 1558-2515. DOI: 10.1109/TASC.2017.2775584.

[4] YUAN, X. and J. WANG. Torque Distribution Strategy for a Front- and Rear-Wheel-Driven Electric Vehicle. *IEEE Transactions on Vehicular Technology*. 2012, vol. 61, iss. 8, pp. 3365–3374. ISSN 1939-9359. DOI: 10.1109/TVT.2012.2213282.

[5] LIU, X., Q. LIN and W. FU. Optimal Design of Permanent Magnet Arrangement in Synchronous Motors. *Energies*. 2017, vol. 10, iss. 11, pp. 1996–1073. ISSN 1996-1073. DOI: 10.3390/en10111700.

[6] PELLEGRINO, G., F. CUPERTINO and C. GERADA. Automatic Design of Synchronous Reluctance Motors Focusing on Barrier Shape Optimization. *IEEE Transactions on Industry Applications*. 2015, vol. 51, iss. 2, pp. 1465–1474. ISSN 1939-9367. DOI: 10.1109/TIA.2014.2345953.

[7] RAMARATHNAM, S., A. K. MOHAMMED, B. BILGIN, A. SATHYAN, H. DADKHAH and A. EMADI. A Review of Structural and Thermal Analysis of Traction Motors. *IEEE Transactions on Transportation Electrification*. 2015, vol. 1, iss. 3, pp. 255–265. ISSN 2332-7782. DOI: 10.1109/TTE.2015.2476478.

[8] MINH, D. B., L. D. HAI, T. L. ANH and V. D. QUOC. Electromagnetic Torque Analysis of SRM 12/8 by Rotor/Stator Pole Angle. *Engineering, Technology & Applied Science Research*. 2021, vol. 11, iss. 3, pp. 255–265. ISSN 7187-7190. DOI: 10.48084/etasr.4168.

[9] MINH, D. B., V. D. QUOC and P. N. HUY. Efficiency Improvement of Permanent Magnet BLDC Motors for Electric Vehicles. *Engineering, Technology & Applied Science Research*. 2021, vol. 11, iss. 5, pp. 7615–7618. ISSN 7187-7190. DOI: 10.48084/etasr.4367.

[10] PELLEGRINO, G., A. VAGATI, P. GUGLIELMI and B. BARBARA. Performance Comparison Between Surface-Mounted and Interior PM Motor Drives for Electric Vehicle Application. *IEEE Transactions on Industrial Electronics*. 2012, vol. 59, iss. 2, pp. 803–811. ISSN 1557-9948. DOI: 10.1109/TIE.2011.2151825.

[11] KOUSALYA, V., R. RAI and B. SINGH. Sliding Model-Based Predictive Torque Control of Induction Motor for Electric Vehicle. *IEEE Transactions on Industry Applications*. 2022, vol. 58, iss. 1, pp. 742–752. ISSN 1939-9367. DOI: 10.1109/TIA.2021.3131973.

[12] SAVARAPU, S., M. QUTUBUDDIN and Y. NARRI. Modified Brain Emotional Controller-Based Ripple Minimization for SVM-DTC of Sensorless Induction Motor Drive. *IEEE Access*. 2022, vol. 10, iss. 1, pp. 40872–40887. ISSN 2169-3536. DOI: 10.1109/ACCESS.2022.3165651.

[13] ZHU, S., W. CHEN, M. XIE, C. LIU and K. WANG. Electromagnetic Performance Comparison of Multi-Layered Interior Permanent Magnet Machines for EV Traction Applications. *IEEE Transactions on Magnetics*. 2018, vol. 54, iss. 11, pp. 1–5. ISSN 1941-0069. DOI: 10.1109/TMAG.2018.2841851.

[14] SAHOO, A. K. and R. K. JENA. Torque Quality Improvement in Induction Motor for Electric Vehicle Application Based on Teamwork Optimization. *Advances in Electrical and Electronic Engineering*. 2022, vol. 20, iss. 4, pp. 359–379. ISSN 1804-3119. DOI: 10.15598/aeee.v20i4.4538.

[15] HWANG, M.-H., J.-H. HAN, D.-H. KIM and H.-R. CHA. Design and Analysis of Rotor Shapes for IPM Motors in EV Power Traction Platforms. *Energies*. 2018, vol. 11, iss. 10, pp. 1–12. ISSN 1996-1073. DOI: 10.3390/en11102601.

About Authors

Vuong DANG QUOC received his Ph.D. degree in 2013 from the Faculty of Applied Sciences at the University of Liege in Belgium. After that he came back to the Hanoi University of Science and Technology in September 2013, where he is currently working as a deputy director of Training Center of Electrical Engineering, School of Electrical and Electronic Engineering, Hanoi, University of Science and Technology. He became an associate professor in 2020. His research domain encompasses modeling of electrical machines and electromagnetic systems by coupling of subproblem methods.

Dinh BUI MINH received his Ph.D. degree in the Department of Electrical Engineering, TU university, in 2014. After that he came back to the Hanoi University of Science and Technology in September 2014. He is currently working as a lecturer at Department of Electrical Engineering, School of Electrical and Electronic Engineering, Hanoi University of Science and Technology. His research domain encompasses modeling of electrical machines by using numerical methods.

Phi DO CHI received his Ph.D. degree in the Department of Electrical Engineering, Hanoi University of Science and Technology, in 2016. He is currently a Dean Electrical-Electronic Engineering Cao Thang Technical College, Ho Chi Minh city, Vietnam. He is Studying in Electrical Engineering, electrical installation skills, design install a Solar or lighting system; ability to operate, assemble, maintain electrical equipment, electrical systems and solve problems related to electricity and equipment in the production.

Hung BUI DUC (corresponding author) received his Ph.D. degree in 2000 from the Faculty of Applied Sciences at the Hanoi University of Science and Technology. After that he came back to the Hanoi University of Science and Technology in September 2001, where he is currently working as a team leader of electrical machines' group, School of Electrical and Electronic Engineering, Hanoi, University of Science and Technology. His research domain encompasses modeling of electrical machines by using numerical methods.